Solar Energy Materials & Solar Cells 245 (2022) 111869

Contents lists available at ScienceDirect

Solar Energy Materials and Solar Cells

journal homepage: www.elsevier.com/locate/solmat

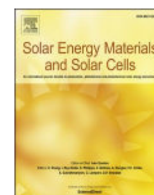

Temporal and spatial atomic layer deposition of Al-doped zinc oxide as a passivating conductive contact for silicon solar cells

Bart Macco [a,*], Mike L. van de Poll [a], Bas W.H. van de Loo [b], Tim M.P. Broekema [a], Saravana B. Basuvalingam [a], Cristian A.A. van Helvoirt [a], Wilhelmus J.H. Berghuis [a], Roel J. Theeuwes [a], Nga Phung [a], Wilhelmus M.M. Kessels [a]

[a] Department of Applied Physics, Eindhoven University of Technology, P.O. Box 513, 5600, MB, Eindhoven, the Netherlands
[b] SALD B.V., Zwaanstraat 1, 5651, CA, Eindhoven, the Netherlands

ARTICLE INFO

Keywords:
Passivating contact
Atomic layer deposition
Surface passivation
Crystalline silicon solar cells
Transparent conductive oxide

ABSTRACT

Recently, stacks consisting of an ultrathin SiO_2 coated with atomic-layer-deposited (ALD) Al-doped zinc oxide (ZnO:Al) have been shown to yield state-of-the-art passivation of *n*-type crystalline silicon surfaces and provide low contact resistivities to n^+-doped Si and poly-Si surfaces. Key for achieving good surface passivation are an intentionally-grown SiO_2 interlayer, an aluminum oxide (Al_2O_3) capping layer and a post-deposition anneal, whereas *n*-type doping of the ZnO is required to achieve a low contact resistivity. In this work, we present the latest results and insights obtained for this contact stack. This includes a study of the minimum required thicknesses of both the ZnO and the Al_2O_3 capping layer to achieve a high passivation level after post-deposition anneal. Also, we provide details on how to remove the Al_2O_3 capping layer selectively from the ZnO:Al after the post-deposition anneal using a pH-controlled wet-etch, such that the ZnO:Al can be contacted by a metal. Whereas previous work was based on lab-scale temporal ALD, in this work we highlight the industrialization potential by demonstrating that these layers can be prepared by spatial ALD, yielding good passivation levels on both undiffused *n*-type and n^+-diffused *c*-Si surfaces. Finally, we demonstrate the capability of ALD to deposit ZnO:Al layers selectively on oxidized regions of an otherwise HF-last treated *c*-Si surface. Such area-selective deposition opens up potential pathways for local, self-aligned contact formation. Altogether, this work provides valuable insights into the working mechanism and practical aspects of ZnO:Al-based passivating contacts.

1. Introduction

So-called passivating contacts have been an immensely popular topic in research, especially over the last decade [1–6]. Many material systems have been studied and passivating contacts can nowadays be found in many commercial solar cells [7]. In conventional homojunction contacts, carrier-selectivity arises from the asymmetric conductivity induced by the highly doped n^+ and p^+ regions within the *c*-Si wafer. This facilitates majority carrier extraction at the metal contact and shields minority carriers from the recombination-active Si-metal contact. Yet, high doping of the *c*-Si wafer comes at the expense of Auger-recombination losses, limiting the open-circuit voltage V_{oc}. Passivating contacts improve upon conventional homojunction contacts by inducing carrier-selectivity from passivating films deposited on the wafer, i.e. they are heterojunctions. This renders high n^+ and p^+ doping of the wafer obsolete and moreover makes sure that there is no recombination-active direct Si-metal contact. Because of this, passivating contact cells typically boast much higher V_{oc} values [1–3].

Many material classes have been explored for passivating contacts, including doped hydrogenated amorphous (*a*-Si:H) and polycrystalline silicon (poly-Si) as well as metal oxides, fluorides and nitrides (referred to here as metal compounds) [1–3]. The main potential benefit of metal compounds over doped Si is their generally higher transparency because of their wide bandgap, enabling less parasitic absorption of light by the contact layers [1,2]. Yet, to date the most efficient cells are still made using doped Si contacts, as doped Si makes up for its limited transparency (so relatively lower short-circuit current density J_{sc}) by having superior surface passivation and majority carrier extraction (hence high V_{oc} and fill factor *FF*) [1]. While likely not a fundamental issue, in practice all metal compound passivating contacts have one or more

* Corresponding author.
E-mail address: b.macco@tue.nl (B. Macco).

https://doi.org/10.1016/j.solmat.2022.111869
Received 16 May 2022; Received in revised form 22 June 2022; Accepted 26 June 2022
Available online 2 July 2022
0927-0248/© 2022 The Authors. Published by Elsevier B.V. This is an open access article under the CC BY license (http://creativecommons.org/licenses/by/4.0/).

drawbacks in this respect, including non-perfect passivation, poor selective carrier extraction, and/or being susceptible to external influences that can impair the contact performance [1]. The latter is caused by a Fermi level that is easily shifted in these typically wide bandgap, intrinsic materials. Because of this, doping of metal compounds is a promising approach to improve selectivity and resilience of the Fermi level to external influences, as also recently proposed by Michel *et al.* [1].

Within this broader context, it is interesting to consider doped ZnO as contact material. As outlined below and in previous work, doped ZnO can enable a hybrid approach between homo- and heterojunction contacts where a n^+-doped Si surface is contacted by a passivating transparent conductive oxide (TCO) [8]. Moreover, being a TCO, it can simultaneously aid in lateral conductivity and antireflection. For the purpose of clarity, the main findings so far are summarized here for this contact material. Specifically, in 2019 our group showed that ALD ZnO/Al_2O_3 stacks can yield excellent passivation on *n*-type *c*-Si, as witnessed by implied V_{oc} levels of 728 mV [9]. While ZnO was not well-known for its surface passivating properties, in that work it was demonstrated that good surface passivation can be achieved provided a few key aspects are taken into account [9]. Firstly, it is prerequisite to form a high-quality SiO_2 interlayer on the *c*-Si wafer prior to ALD of ZnO, as it appears that ALD ZnO does not naturally form a high-quality interfacial SiO_2 interface on *c*-Si. Secondly, the presence of an ALD Al_2O_3 capping layer is essential to prevent effusion of hydrogen from the stack during an anneal at 400–450 °C that is necessary to activate the passivation. Finally, doping of the ZnO can enhance the *field-effect* passivation, since doping reduces the work function of the ZnO and thereby results in more downward band bending at the *c*-Si surface [9].

In subsequent work, we demonstrated that this ZnO-based stack can not only provide surface passivation, but can also yield a low contact resistivity to n^+-diffused surfaces and poly-Si(*n*) contacts, as well as providing a low sheet resistance and good optical incoupling into *c*-Si [8]. In addition to demonstrating the contact properties, many insights were gained in the working principle of this contact stack. Doping of both the ZnO:Al and *n*-type *c*-Si was shown to be required for achieving low contact resistivities down to 15 mΩcm^2. The anneal step was found to lead to optimal passivation at temperatures around 450–500 °C, where higher annealing temperatures lead to rapid loss of passivation. The latter was shown by transmission electron microscopy (TEM) imaging to originate from break-up of the interfacial SiO_2 at high annealing temperatures. The anneal step also enables significant improvements in the carrier mobility (by approximately 50%) of the ZnO:Al (up to 38 cm^2/Vs), such that resistivity and transparency levels typical to those of indium-based TCOs are reached. Specifically, depending on the doping level, resistivity values well below 1 mΩcm and down to 0.5 mΩcm were achieved, while optical modelling show a J_{sc} potential in excess of 42 mA/cm^2 (ignoring front metallization) [8]. Importantly, this improvement is only observed when an Al_2O_3 capping layer is present, whereas ZnO:Al films without an Al_2O_3 capping layer degrade strongly upon annealing. Similar to surface passivation, it is thought that passivation of defects in the ZnO by hydrogen play an important role in this mobility improvement. Moreover, TEM imaging elucidated two more effects of annealing that can contribute to an improved carrier mobility. Firstly, upon annealing the grain size increases due to coarsening. Secondly, the Al dopants that originally are present in planes due to the ALD supercycle deposition approach become more isotropically spread over the film [10].

In this work, we present the latest results and insights obtained for this contact stack. Firstly, the upscaling potential is highlighted by demonstrating that the ZnO:Al/Al_2O_3 stack can also be prepared by spatial ALD, yielding passivation levels on both undiffused *n*-type and n^+-diffused *c*-Si surfaces that are similar to those obtained by temporal ALD. Furthermore, we demonstrate that both the ZnO and Al_2O_3 layers can be made significantly thinner than in previous studies without significant loss of passivation. Also, we provide details on a pH-controlled wet-etch that was developed to remove the Al_2O_3 selectively from the ZnO:Al after the post-deposition anneal, such that the ZnO:Al can be contacted by a metal. Finally, we demonstrate the capability of ALD to deposit ZnO:Al layers selectively on oxidized regions of an otherwise HF-last treated *c*-Si surface. Such area-selective deposition opens up potential pathways for local, self-aligned contact formation.

2. Experimental section

2.1. Substrates and pre-treatments

In this work, two types of *c*-Si substrates were used for the preparation of symmetrical lifetime samples. The first type are double-side mirror-polished floatzone (FZ) *c*-Si wafers, which are 285 μm-thick and are *n*-type doped with a resistivity of 3 Ωcm. Secondly, to evaluate the passivation performance on n^+-diffused surfaces, Czochralski (CZ) *c*-Si wafers (*n*-type, 3 Ωcm, 185 μm-thick) with a 137 Ω/sq n^+-emitter prepared by $POCl_3$ diffusion in a tube furnace were used. These wafers featured an interfacial oxide either grown by Radio Corporation of America (RCA) cleans or by UV/O_3 oxidation. UV/O_3 oxidation was performed for 30 min at room temperature in a Novascan PSD Series UV Ozone Cleaner, directly after a 1% HF dip for 1 min and rinse in DI water.

2.2. Film preparation

Both temporal and spatial ALD were used to prepare the ZnO:Al and Al_2O_3 layers in this work. For both types of ALD, diethylzinc (DEZ) and dimethylaluminumisopropoxide (DMAI) were used as the zinc and aluminum precursors, respectively, and H_2O as co-reactant. For Al-doping of the ZnO, DMAI was used as it is a more efficient doping precursor compared to trimethylaluminum (TMA) [11]. On the temporal ALD tool, the DMAI and DEZ bubblers were kept at 50 and 25 °C, while on the spatial ALD tool they were kept at 25 and 35 °C, respectively.

For Al-doping of the ZnO:Al both the so-called supercycle and co-injection approaches were used. The supercycle method was used for temporal ALD, where a doped film is deposited by repeating a pattern of an integer *n* cycles of ZnO and one Al_2O_3 cycle. In this approach, the doping level can be controlled accurately by varying the integer *n*. The co-injection method was used for spatial ALD, where the Zn and Al precursors are injected simultaneously every cycle and the doping level can be controlled by the mixing ratio of the two (or more) precursors.

Temporal ALD was performed in an Oxford Instruments OpAL™ reactor at a table temperature of 200 °C, similarly as described in our previous work [8]. The dose times were 60 ms for both DEZ and DMAI and 200 ms for H_2O. A 6 s purge was used after the DEZ and DMAI steps, while a 10 s purge was used after the H_2O dose. Spatial ALD was performed at atmospheric pressure in an R&D tool of the company SALD (former SoLayTec) at 230 °C. This tool allows for single-sided deposition and in-line atmospheric pressure processing. Moreover, it is configurable for both co-injection and supercycles, where in this work we focused on co-injection. The system consists of a substrate table that is moved back and forth underneath gas nozzles with a velocity of 500 mm/s. The gas nozzles are supplied with precursors from heated canisters through bubbling with N_2, while the H_2O co-reactant is supplied from an evaporator. Nitrogen gas curtains were used to prevent intermixing of the H_2O and precursor gases present in the distinct precursor zones. For Al-doping of the ZnO, DMAI and DEZ were co-dosed using N_2 flows of 0.5 slm and 2.0 slm, respectively. XPS showed successful incorporation of Al (1.5 at. %) and the carrier density was raised from 0.3×10^{20} to 1.6×10^{20} cm^{-3} with respect to intrinsic ZnO (iZnO).

Silicon nitride (SiN_x) was tested as alternative capping layer and was deposited by plasma-enhanced chemical vapor deposition (PE-CVD) using an inductively coupled plasma tool (PlasmaLab 100 ICP) from Oxford Instruments, similarly as described in our earlier works [12,13]. The substrate temperature was kept at 200 °C, where helium backflow

was applied to the sample to ensure a good thermal contact between the sample holder and the substrate. Nitrogen and silane were injected with a flow of 24 and 16 sccm, respectively, and a plasma power of 500W was applied. The pressure was actively controlled by an automated pressure controller (APC) at 12 mTorr. From XPS, the Si:N ratio of these films was determined to be 1.3.

Post-deposition forming gas anneals (FGA, 10/90H_2/N_2) were performed in a Jipelec rapid thermal anneal furnace. All anneals were done consecutively for 5 min at temperatures ranging from 300 to 650 °C at 50 °C increments. Selective wet-etching of Al_2O_3 from the ZnO(:Al) stack was done using a 0.1 M solution of Na_2CO_3 at 60 °C of which the pH was controlled to 11.8 by KOH dripping, similarly as done in our earlier work and in the work of Sun et al. [8,14].

2.3. Analysis

The passivation quality and the implied open-circuit voltage (iV_{oc}) were evaluated using a Sinton WCT-120TS lifetime tester. Spectroscopic ellipsometry (SE) was used for determination of the optical constants and thicknesses of ALD layers. The optical constants of ZnO:Al were modeled using a combination of a Tauc-Lorentz and a Drude oscillator, while a PSEMI-M0 model was used for undoped ZnO samples. The latter was done since the PSEMI-M0 model is better able to account for the sharper transition in absorption around the bandgap energy that is typical of undoped films. The Drude oscillator was used to evaluate the carrier density in the film [15]. The Al_2O_3 and SiN_x dielectrics were modeled in their transparent regions (i.e. below the band gap) using a Cauchy function. The film composition was evaluated by X-ray photoelectron spectroscopy (XPS) using a Thermo Scientific KA1066 spectrometer.

3. Results and discussion

The passivation quality of spatial ALD ZnO:Al/Al_2O_3 stacks was evaluated on symmetrical lifetime samples on both undiffused FZ and n^+-diffused (137 Ω/sq) CZ c-Si(n) wafers. As can be seen in Fig. 1, on both substrate types the passivation in the as-deposited state is poor, irrespective of the ZnO:Al doping level. Note that for the n^+-diffused wafers the iV_{oc} in the as-deposited state is significantly higher than for the undiffused wafers, since the n^+-diffusion helps shield minority carriers (i.e. holes) from the poorly passivated surface [3]. Upon annealing, the passivation level improves significantly for both substrate types, with an optimum around 400–450 °C of annealing, resulting in iV_{oc} values up to 718 and 701 mV for undiffused and n^+-diffused wafers, respectively. For annealing temperatures of 500 °C and higher, the passivation quality degrades rapidly. The same trend was observed in our previous work on temporal ALD ZnO:Al contacts, where a TEM study suggested that roughening and disordering of the interfacial SiO_2 at high annealing temperatures contributes to this loss of passivation [8].

On undiffused wafers, the doped ZnO:Al sample reaches an iV_{oc} value of 718 mV, which is slightly better than the 711 mV obtained for iZnO. Also in our previous work on passivation by temporal ALD ZnO, it was found that the passivation level consistently improves slightly for increasing doping levels of the ZnO contacts. This was attributed to a change in interfacial band bending induced by the quickly diminishing work function (WF) of the ZnO contact upon stronger degenerate doping, which was supported by band structure simulations [9]. Presumably, the well-passivated interfacial oxide helps reduce Fermi-level pinning such that the lower WF for doped films also effectively translates to more downward band bending at the c-Si interface. On the n^+-diffused surfaces, no significant difference in the passivation level is observed between the iZnO and ZnO:Al samples, both of which reach an iV_{oc} of (700 ± 2) mV. Although hard to pinpoint exactly from this dataset, plausible explanations include (1) that the carrier population at the c-Si interface is more strongly dictated by the n^+ doping of the c-Si rather than the ZnO:Al doping level (and hence WF) as compared to undiffused c-Si(n) wafers and (2) that for these samples any relatively small differences in surface recombination have a less pronounced effect on the iV_{oc}, as Auger recombination in the highly-doped n^+-region plays a role as well. Specifically, using EDNA 2 calculator the J_0 due to Auger recombination in the highly-doped has been estimated at 15 fA/cm^2, which is on the same order as the surface recombination (see next paragraph). Also, this additional (Auger) recombination induced by n^+ doping of the c-Si subsurface is the most likely reason why lower iV_{oc} values are obtained as compared to undiffused surfaces.

Fig. 2 shows an overview of the passivation level, expressed as the recombination current density J_0 (fA/cm^2), of common passivation schemes on n^+-doped-surfaces on a variety of emitter sheet resistances. The comparison includes the spatial ALD ZnO(:Al)/Al_2O_3 stacks from

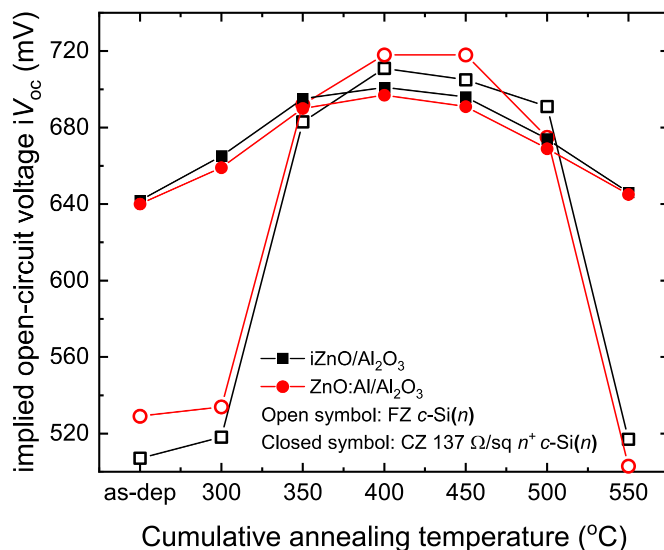

Fig. 1. iV_{oc} values for SiO_x/ZnO(:Al)/Al_2O_3 stacks prepared by spatial ALD on undiffused FZ and n^+-diffused CZ c-Si(n) wafers with RCA and UV/O_3 SiO_2 layers, respectively. The ZnO and Al_2O_3 films had a thickness of 30 nm. Consecutive annealing steps were performed for 5 min in forming gas ambient. The corresponding J_0 values on n^+-diffused surfaces can be found in the Supplementary information, Fig. S1.

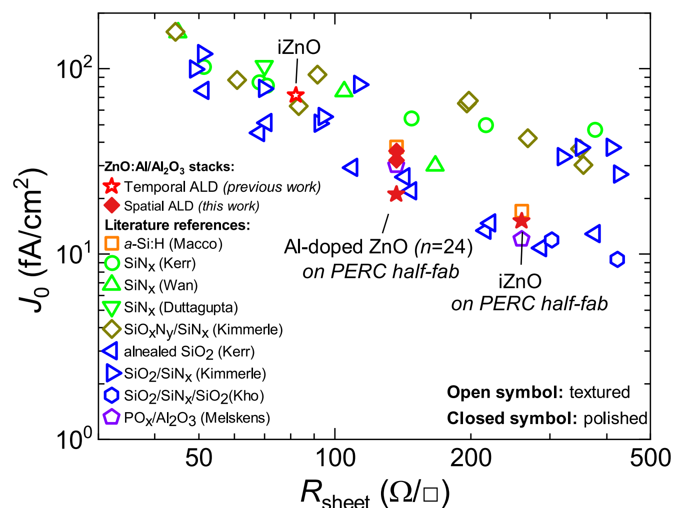

Fig. 2. Overview of the passivation quality of a range of passivation schemes on n^+-diffused surfaces. The overview includes the spatial ALD ZnO(:Al)/Al_2O_3 from this work and temporal ALD ZnO(:Al)/Al_2O_3 stacks from our previous work [8], as well literature values for common passivation schemes based on (combinations of) a-Si:H, SiN_x, SiO_2, Al_2O_3, and PO_x [12,17–23]. For the ZnO-based results, a UV/O_3 oxide was employed.

this work as well as temporal ALD results from previous work, where some datapoints were acquired on PERC half-fabricate cells [8]. As can be seen, the ZnO-based contacts generally show a high level of passivation. The spatial ALD films specifically also give low J_0 values down to 32 fA/cm^2 on the 137 Ω/sq surface, yet are not completely on par with the result obtained for temporal ALD on the PERC half-fabricate cells. It should however be stressed that this might not be due to a fundamental difference between temporal and spatial ALD, but could also arise from the fact that in this specific case the temporal ALD ZnO:Al was more highly doped. Specifically, the temporal ALD sample prepared with a supercycle ratio $n = 24$ has a higher carrier density N_e of 3.3×10^{20} cm^{-3} as compared to 1.6×10^{20} cm^{-3} for spatial ALD.

As mentioned in the introduction, the Al_2O_3 capping layer is crucial for achieving surface passivation as it prevents the effusion of hydrogen from the passivation stack upon thermal annealing [9]. However, thus far all passivation results were obtained for relatively thick Al_2O_3 capping layers, i.e. 30 nm. In this work, the thickness required for achieving good passivation was investigated in detail. Such insight is relevant for implementation of the passivating stack, since the Al_2O_3 layer is *sacrificial*, i.e. every nanometer of Al_2O_3 that has been deposited also has to be etched of after the post-deposition anneal. Fig. 3 shows the passivation performance of spatial ALD 30 nm iZnO/*x* nm Al_2O_3 passivation stacks as a function of annealing temperature. For 0 and 2 nm of Al_2O_3 no appreciable passivation is observed. Importantly, for both these samples approximately millimeter-sized specks started to appear after forming gas annealing at 500 °C, while the films were completely removed after annealing at 550 °C. For annealing below 500 °C, such removal of the film and/or degradation was not observed. This suggests that the Al_2O_3 capping layer not only plays a key role for hydrogenation but also helps prevent etching of the ZnO during forming gas annealing, provided the Al_2O_3 is sufficiently thick and closed. For 4 nm of Al_2O_3 capping layer, some activation of the surface passivation is observed, reaching modest iV_{oc} values of around 600 mV. For Al_2O_3 capping layers of 8 nm and thicker, equally good passivation is observed for annealing temperatures up to 450 °C. This demonstrates that for reaching a high level of passivation, the Al_2O_3 capping layer can be significantly thinner than the previously-employed thickness of 30 nm.

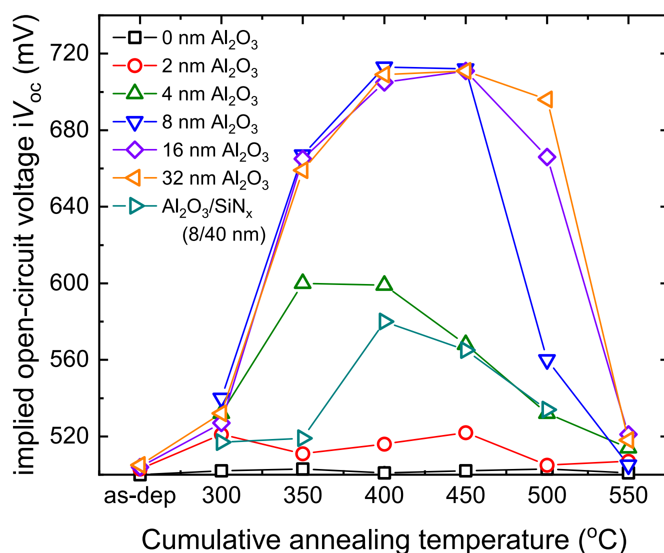

Fig. 3. Influence of the thickness of the Al_2O_3 capping layer thickness on the passivation quality for 30 nm iZnO/*x* nm Al_2O_3 stacks prepared by spatial ALD on undiffused FZ c-Si(n) wafers with an RCA SiO_2 layer. To evaluate the possibility of using SiN_x as an alternative capping layer, 30 nm iZnO/40 nm SiN_x stacks and 30 nm iZnO/8 nm Al_2O_3/40 nm SiN_x stacks were prepared. For the iZnO/SiN_x sample the iV_{oc} could not be determined reliably due to extremely poor passivation. Consecutive annealing steps were performed for 5 min in forming gas ambient.

Yet, upon annealing at 500 °C it is observed that a thicker capping layer does help to mitigate the loss of passivation, presumably by preventing the effusion of hydrogen more effectively. After annealing at 550 °C, the passivation is effectively lost for all Al_2O_3 capping layer thicknesses, which is thought to originate from aforementioned disintegration of the interfacial oxide as observed in TEM [8].

Also 40 nm of PE-CVD SiN_x was tested as an alternative capping layer, either directly on iZnO or in a 8 nm Al_2O_3/SiN_x stack [24] Our experiments showed very low lifetimes around 1 μs for the iZnO/SiN_x stack, which could not be recovered by post-deposition annealing (not shown). For the 8 nm Al_2O_3/SiN_x stack, annealing leads to only slight surface passivation, where the achieved iV_{oc} values are well below 600 mV. The low passivation could potentially be due to plasma-induced damage by the SiN_x deposition as has been observed for various systems, including *a*-Si:H and SiO_2/poly-Si passivation layers, and has often been attributed to photons and ions [25–29]. Though still a topic of study, this does show that the Al_2O_3 capping layer is not easily replaced by other common capping layers.

Furthermore, it was found that the ZnO layer in the ZnO/Al_2O_3 stack can be made relatively thin, without significant loss of passivation. As can be seen in Fig. 4, the passivation quality only decreases slightly when going from 75 nm thick ZnO (the optimal for antireflection) down to 5 nm. For such thin layers, one of the potential reasons for reduced passivation could be the fact that the film is not closed. Indeed, in earlier work it was shown that ALD ZnO grows in a so-called island mode, where it takes close to 10 nm for coalescence of these islands (i.e. film closure) to complete [26]. For the 0 nm ZnO data point (i.e. only SiO_2/Al_2O_3) the passivation level is relatively low. While such a stack should yield a high level of chemical passivation, the lower passivation level can partly originate from the negative fixed charge in such a stack which is better suited for passivating *p*-type *c*-Si surfaces [30]. Yet, the main difference is thought to originate from the employed anneal temperature of 450 °C which is optimized for the ZnO contacts, whereas the best passivation for Al_2O_3 layers themselves is typically found using a 400 °C annealing temperature.

For selective etching of the Al_2O_3 from the ZnO:Al layers, a procedure based on the work of Sun et al. was developed [14]. This pH-controlled selective wet-etch is based on a 0.1 M Na_2CO_3 solution at 60 °C of which the pH is raised to 11.8 by KOH dripping. As shown in

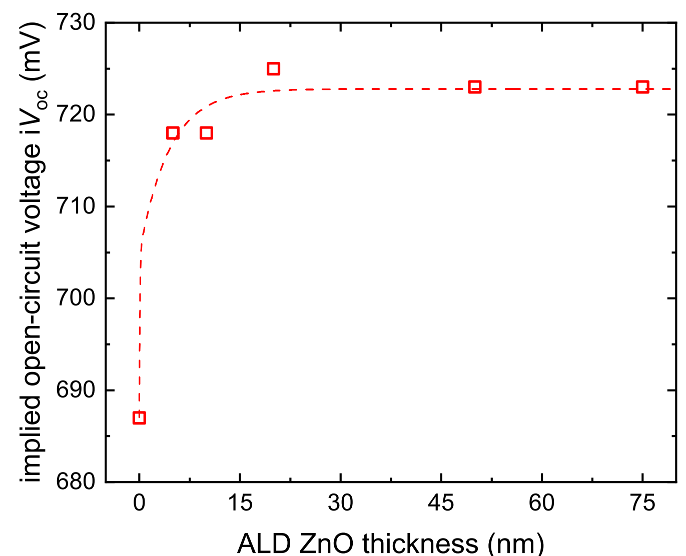

Fig. 4. Influence of the thickness of the iZnO layer thickness on the passivation quality for iZnO/30 nm Al_2O_3 stacks prepared by temporal ALD on FZ c-Si(n) substrates that feature an SiO_2 interlayer prepared by UV/O_3 oxidation. The samples were subjected to a post-deposition anneal in forming gas ambient at 450 °C for 30 min. The dashed line is a guide to the eye.

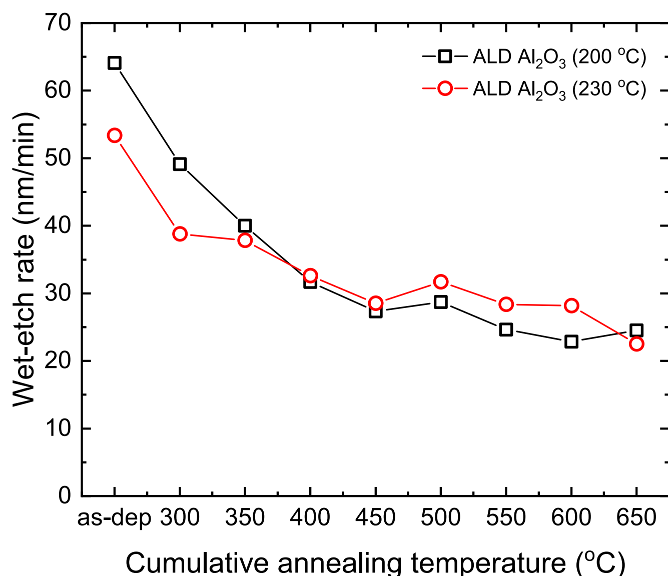

Fig. 5. Influence of annealing on the wet etch rate of Al_2O_3 in a 0.1 M solution of Na_2CO_3 (60 °C, pH = 11.8 by KOH dripping). ALD Al_2O_3 films were prepared by temporal ALD at 200 and 230 °C. Consecutive annealing steps were performed for 5 min in forming gas ambient. The etch rate was determined by spectroscopic ellipsometry. It was verified that both ZnO and SiN_x are not etched by this solution.

Fig. 5, very high etch rates for Al_2O_3 can be achieved with this etching solution, while no appreciable etching of ZnO occurs. Importantly, the etch rate depends on the deposition temperature and decreases strongly after post-deposition annealing. Specifically, ALD Al_2O_3 prepared at 200 °C is etched faster than Al_2O_3 prepared at 230 °C. Upon annealing the etch rates decrease and converge for annealing temperatures of 350 °C and higher.

This reduction in wet-etch rate upon annealing is reminiscent of SiN_x which becomes much more resistant to etching in hydrofluoric acid after high temperature annealing [31]. This was attributed to densification and release of H from the layer, resulting in more strong Si–N bonds. Also the Al_2O_3 layers studied in this work densify significantly upon annealing, as shown in Fig. 6. The thickness of the Al_2O_3 layers decreases upon annealing, which is accompanied by an increase in refractive index n. The Al_2O_3 films prepared at 200 °C have a slightly lower refractive index as compared to films prepared at 230 °C. Also, the films prepared at 200 °C lose relatively more thickness, specifically a little over 9% after annealing at 600 °C as compared to close to 6% for films prepared at 230 °C. Importantly, even though the reduction in wet-etch rate upon annealing is concomitant with densification, the wet-etch rate of the films prepared at 200 and 230 °C is approximately equal after annealing temperatures of 350 °C and higher, while the films prepared a 230 °C still have a higher refractive index.

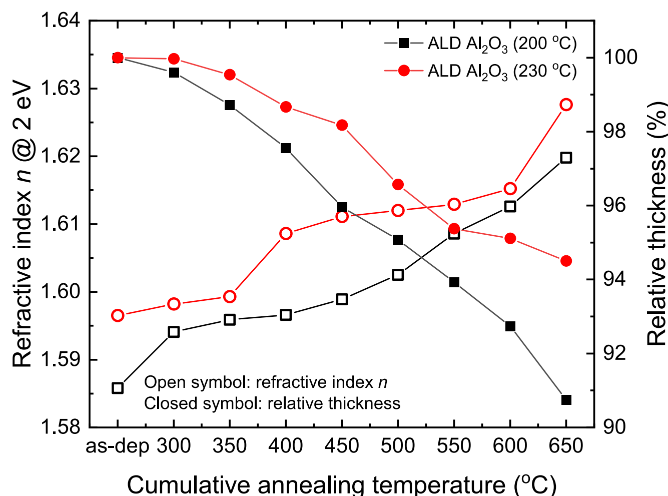

Fig. 6. Change in refractive index n and relative thickness of Al_2O_3 films upon post-deposition annealing as determined from spectroscopic ellipsometry. ALD Al_2O_3 films were prepared by temporal ALD at 200 and 230 °C. Consecutive annealing steps were performed for 5 min in forming gas ambient.

3.1. Area-selective ALD of ZnO:Al

Another important aspect when implementing these ZnO-based contacts is the fact that film growth, and specifically the nucleation, depends strongly on the surface preparation of the *c*-Si wafer. As can be seen in the top panel of Fig. 7, on HF-last *c*-Si surfaces it takes approximately 35 ALD cycles for iZnO to nucleate, while iZnO readily nucleates on an RCA-prepared SiO_2 surface. With a growth-per-cycle (GPC) in the steady-growth regime of 0.18 nm for ZnO, this means that for an identical number of cycles, the resulting film will be about 7 nm thinner on HF-last surfaces than on SiO_2 surfaces. This nucleation delay is thought to originate from a lower reactivity of the DEZ precursor towards the relatively inert Si–H terminated surface, as compared to the hydroxyl groups found on an oxide surface. This statement is motivated by earlier work of Mameli *et al.*, where we already showed that ALD ZnO from the reactants DEZ and H_2O has a strong nucleation delay on Si–H terminated *a*-Si:H layers, while ZnO nucleates readily on intentionally oxidized a-Si:H [32]. Density functional theory calculations indicated that a lack of reactivity of DEZ to the relatively inert Si–H surface groups stands at the basis of this nucleation delay. Specifically, while the chemisorption of DEZ on surface Si–H and Si–OH groups is exothermic in both cases with an energy gain of 0.98 and 1.25 eV, respectively, there is a much stronger activation energy on Si–H surfaces (1.16 eV) as compared to Si–OH surfaces (0.81 eV). Importantly, it was excluded that oxidation of the Si–H surface during H_2O exposure in the ALD cycle is the reason for loss of selectivity as this process is much slower. This is in line with the common notion that HF-dipped *c*-Si surfaces are relatively resilient to oxidation in ambient conditions.

Mameli et al. leveraged this surface-dependent nucleation effect to grow ZnO selectively on *a*-Si:H surfaces that were oxidized locally [32]. Such an approach is often coined area-selective ALD (AS-ALD), a field that is considered an upcoming enabling technology in the semiconductor industry for bottom-up fabrication of nanostructures, yet

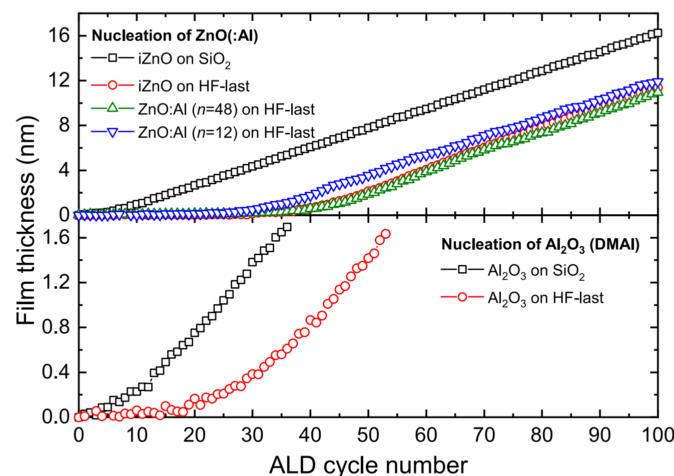

Fig. 7. Nucleation curves of temporal ALD ZnO:Al (top panel) and Al_2O_3 (bottom panel) on H-terminated Si surfaces (labeled HF-last) and Si surfaces with an SiO_2 layer prepared by RCA cleans. The film thicknesses were tracked *in-situ* by spectroscopic ellipsometry.

likely less well-known in the PV community [33]. Since this similar effect is observed on *c*-Si, in principle it can be used to grow ALD ZnO area-selectively on an HF-wafer that is oxidized locally, or conversely an oxidized wafer which is HF-treated locally. Here, we validate the former approach by exposing an HF-treated *c*-Si wafer to an ICP O_2 plasma for 4 s through a mask in the temporal ALD reactor. Subsequently, the mask was removed and 60 ALD iZnO cycles (nominal thickness of 10 nm) and 100 cycles ALD Al_2O_3 (nominal thickness of 8 nm) were performed. After ALD, the masked pattern was clearly visible to the naked eye. On the O_2 plasma-treated surface, ellipsometry measurements confirmed that this results in a near nominal stack thickness of 9.2/7.9 nm iZnO/Al_2O_3. The iZnO thickness was markedly lower on the non-treated area, specifically the iZnO/Al_2O_3 stack was 3.3/8.6 nm thick. This is in line with the nucleation delay observed on HF-last surfaces and confirms that approximately 6 nm of iZnO can be grown selectively on SiO_2-terminated surfaces before film growth starts on HF-last surfaces. As was shown in Fig. 4, such a thickness is sufficient to have a well-passivating ZnO layer on the SiO_2-terminated area. Although a specific cell implementation or process flow of such area-selective ALD of ZnO is not directly evident, it does open up a potential innovative integration pathway for these ALD contacts. Especially since ALD ZnO only yields passivation on thin interfacial silicon oxides but not on HF-last surfaces, it can be advantageous to grow ALD ZnO only on predefined SiO_2 areas in a self-aligned manner. Yet, since doping of the ZnO is a strong prerequisite to form low-Ohmic contacts to *c*-Si, such approach would fail if the doping step in the supercycle would lead to nucleation on the HF-last surfaces. For example, ALD Al_2O_3 grown from TMA and H_2O - probably the most widely adopted ALD process in the PV industry - is known to nucleate readily on HF-last surfaces. Hence, using TMA to dope ZnO:Al in a supercycle manner should lead to rapid loss of selective deposition. Here we show that the less reactive DMAI precursor used in this work also has an appreciable nucleation delay on HF-last surfaces and can thus be used to dope the ZnO:Al without significant loss of area-selectivity. As can be seen in the bottom panel of Fig. 7, Al_2O_3 grown by DMAI and H_2O has no appreciable nucleation delay on an SiO_2 surface, while a delay of almost 20 cycles is present on the HF-last surface. The top panel of Fig. 7 shows the nucleation delay on HF-last *c*-Si of ZnO:Al prepared using supercycle ratios 12 and 48. For a supercycle ratio of 48, the nucleation behavior is very similar as for iZnO. This would point to negligible if any reduction of the selectivity by the Al-doping step, albeit that the first Al-doping cycle is performed only after 24 ALD ZnO cycles, which is close to the nucleation delay itself of approximately 35 cycles. For the $n = 12$ sample the nucleation delay is slightly reduced to approximately 27 cycles, at which point the surface has already experienced two Al-doping cycles (after ZnO cycles 6 and 18). This demonstrates that the DMAI step reduces the selectivity only slightly, even for extremely highly doped films prepared with $n = 12$.

4. Conclusions

ZnO-based contacts present an interesting approach for fabricating *c*-Si solar cell contacts, as they can combine high levels of surface passivation and low-Ohmic contacting, as well as lateral conductivity and antireflection. In this work, we provide the latest insights gained into both the practical aspects and working mechanism of this contacting approach. Firstly, it has been shown that spatial ALD is a viable method to prepare the contact stack with passivation performance on a similar level as found in earlier studies using lab-scale temporal ALD, underlining the potential for industrialization. Additionally, it was found that the thickness of the ZnO and Al_2O_3 layers can be reduced considerably from 75 to 30 nm in previous studies to at least 5 and 8 nm, respectively, without significant loss of passivation quality. Selective etching of the sacrificial Al_2O_3 from the ZnO was shown to be fast and effective in a basic Na_2CO_3 solution. Although the wet-etch rate of Al_2O_3 drops significantly after post-deposition annealing as the layer densifies, still practically high etch rates over 20 nm/min were achieved. Yet, the influence of etching in a Na_2CO_3 solution on the solar cell process flow has not been investigated yet and will be left for future work. Finally, since both ALD ZnO and Al_2O_3 exhibit a strong nucleation delay on HF-treated surfaces, ZnO:Al layers can be grown area-selectively on a locally oxidized region of HF-treated wafers, opening up potential innovative integration pathways for this contact material.

CRediT authorship contribution statement

Bart Macco: Writing – original draft, Visualization, Supervision, Project administration, Methodology, Investigation, Funding acquisition, Formal analysis, Data curation, Conceptualization. **Mike L. van de Poll:** Writing – review & editing, Investigation. **Bas W.H. van de Loo:** Writing – review & editing, Investigation. **Tim M.P. Broekema:** Writing – review & editing, Investigation. **Saravana B. Basuvalingam:** Writing – review & editing, Investigation. **Cristian A.A. van Helvoirt:** Investigation. **Wilhelmus J.H. Berghuis:** Writing – review & editing, Investigation. **Roel J. Theeuwes:** Writing – review & editing. **Nga Phung:** Writing – review & editing, Investigation. **Wilhelmus M.M. Kessels:** Writing – review & editing, Supervision, Project administration, Funding acquisition.

Declaration of competing interest

The authors declare that they have no known competing financial interests or personal relationships that could have appeared to influence the work reported in this paper.

Data availability

Data will be made available on request.

Acknowledgements

The authors acknowledge B. Krishnamoorty, J.J.L.M. Meulendijks, C. O. van Bommel, C.A.A. van Helvoirt and J.J.A. Zeebregts for their technical support. J.F.W. Maas is acknowledged for assistance in setting up and characterizing the spatial ALD ZnO:Al process. We acknowledge financial support for this research from the Top consortia for Knowledge and Innovation (TKI) Solar Energy program “PERCspective” (TEUE119005) of the Ministry of Economic Affairs of The Netherlands. The work of B. Macco was supported by The Netherlands Organization for Scientific Research under the Dutch TTW-VENI Grant 16775 and TTW-OTP Grant 18697.

Appendix A. Supplementary data

Supplementary data to this article can be found online at https://doi.org/10.1016/j.solmat.2022.111869.

References

[1] J. Ibarra Michel, J. Dréon, M. Boccard, J. Bullock, B. Macco, Carrier-selective contacts using metal compounds for crystalline silicon solar cells, Prog. Photovoltaics Res. Appl. (2022) 1–34, https://doi.org/10.1002/pip.3552.

[2] J. Melskens, B.W.H. van de Loo, B. Macco, L.E. Black, S. Smit, W.M.M. Kessels, Passivating contacts for crystalline silicon solar cells: from concepts and materials to prospects, IEEE J. Photovoltaics 8 (2018) 373–388, https://doi.org/10.1109/JPHOTOV.2018.2797106.

[3] T.G. Allen, J. Bullock, X. Yang, A. Javey, S. De Wolf, Passivating contacts for crystalline silicon solar cells, Nat. Energy (2019), https://doi.org/10.1038/s41560-019-0463-6, 2–3.

[4] K. Gao, Q. Bi, X. Wang, W. Liu, C. Xing, K. Li, D. Xu, Z. Su, C. Zhang, J. Yu, D. Li, B. Sun, J. Bullock, X. Zhang, X. Yang, Progress and future prospects of wide-bandgap metal-compound-based passivating contacts for silicon solar cells, Adv. Mater. (2022), 2200344, https://doi.org/10.1002/adma.202200344.

[5] M. Hermle, F. Feldmann, M. Bivour, J.C. Goldschmidt, S.W. Glunz, Passivating contacts and tandem concepts: approaches for the highest silicon-based solar cell efficiencies, Appl. Phys. Rev. 7 (2020), 021305, https://doi.org/10.1063/1.5139202.

[6] B. Macco, B.W.H. van de Loo, W.M.M. Kessels, Atomic Layer Deposition for High Efficiency Crystalline Silicon Solar Cells, Wiley, 2017.

[7] Y. Chen, D. Chen, C. Liu, Z. Wang, Y. Zou, Y. He, Y. Wang, L. Yuan, J. Gong, W. Lin, X. Zhang, Y. Yang, H. Shen, Z. Feng, P.P. Altermatt, P.J. Verlinden, Mass production of industrial tunnel oxide passivated contacts (i-TOPCon) silicon solar cells with average efficiency over 23% and modules over 345 W, Prog. Photovoltaics Res. Appl. (2019) 3180, https://doi.org/10.1002/pip.3180.

[8] B. Macco, B.W.H. van de Loo, M. Dielen, D.G.J.A. Loeffen, B.B. van Pelt, N. Phung, J. Melskens, M.A. Verheijen, W.M.M. Kessels, Atomic-layer-deposited Al-doped zinc oxide as a passivating conductive contacting layer for n^+-doped surfaces in silicon solar cells, Sol. Energy Mater. Sol. Cells 233 (2021), 111386, https://doi.org/10.1016/j.solmat.2021.111386.

[9] B.W.H. van de Loo, B. Macco, J. Melskens, W. Beyer, W.M.M. Kessels, Silicon surface passivation by transparent conductive zinc oxide, J. Appl. Phys. 125 (2019), 105305, https://doi.org/10.1063/1.5054166.

[10] Y. Wu, A.D. Giddings, M.A. Verheijen, B. Macco, T.J. Prosa, D.J. Larson, F. Roozeboom, W.M.M. Kessels, Dopant distribution in atomic layer deposited ZnO: Al films visualized by transmission electron microscopy and atom probe tomography, Chem. Mater. 30 (2018), https://doi.org/10.1021/acs.chemmater.7b03501.

[11] Y. Wu, S.E. Potts, P.M. Hermkens, H.C.M. Knoops, F. Roozeboom, W.M.M. Kessels, Enhanced doping efficiency of Al-doped ZnO by atomic layer deposition using dimethylaluminum isopropoxide as an alternative aluminum precursor, Chem. Mater. 25 (2013) 4619–4622, https://doi.org/10.1021/cm402974j.

[12] B. Macco, J. Melskens, N.J.N.J. Podraza, K. Arts, C. Pugh, O. Thomas, W.M. M. Kessels, Correlating the silicon surface passivation to the nanostructure of low-temperature a-Si:H after rapid thermal annealing, J. Appl. Phys. 122 (2017), 035302, https://doi.org/10.1063/1.4994795.

[13] W.J.H. Berghuis, J. Melskens, B. Macco, R.J. Theeuwes, L.E. Black, M.A. Verheijen, W.M.M. Kessels, Excellent surface passivation of germanium by *a*-Si:H/Al_2O_3 stacks, J. Appl. Phys. 130 (2021), 135303, https://doi.org/10.1063/5.0064808.

[14] K.G. Sun, Y.V. Li, D.B. Saint John, T.N. Jackson, pH-controlled selective etching of Al_2O_3 over ZnO, ACS Appl. Mater. Interfaces 6 (2014) 7028–7031, https://doi.org/10.1021/am501912q.

[15] H.C.M. Knoops, B.W.H. van de Loo, S. Smit, M.V. Ponomarev, J.-W. Weber, K. Sharma, W.M.M. Kessels, M. Creatore, Optical modeling of plasma-deposited ZnO films: electron scattering at different length scales, J. Vac. Sci. Technol. A Vacuum, Surfaces, Film. 33 (2015), 021509, https://doi.org/10.1116/1.4905086.

[17] M.J. Kerr, J. Schmidt, A. Cuevas, J.H. Bultman, Surface recombination velocity of phosphorus-diffused silicon solar cell emitters passivated with plasma enhanced chemical vapor deposited silicon nitride and thermal silicon oxide, J. Appl. Phys. 89 (2001) 3821–3826, https://doi.org/10.1063/1.1350633.

[18] S. Duttagupta, F. Ma, B. Hoex, T. Mueller, A.G. Aberle, Optimised antireflection coatings using silicon nitride on textured silicon surfaces based on measurements and multidimensional modelling, Energy Proc. 15 (2012) 78–83, https://doi.org/10.1016/j.egypro.2012.02.009.

[19] Y. Wan, D. Yan, A. Cuevas, K.R. McIntosh, Influence of the NH_3:SiH_4 ratio and surface morphology on the surface passivation of phosphorus-diffused *c*-Si by PECVD SiN_x, in: 2014 IEEE 40th Photovolt. Spec. Conf., IEEE, 2014, pp. 3317–3321, https://doi.org/10.1109/PVSC.2014.6925644.

[20] A. Kimmerle, M. Momtazur Rahman, S. Werner, S. Mack, A. Wolf, A. Richter, H. Haug, Precise parameterization of the recombination velocity at passivated phosphorus doped surfaces, J. Appl. Phys. 119 (2016), 025706, https://doi.org/10.1063/1.4939960.

[21] T.C. Kho, K.C. Fong, M. Stocks, K. McIntosh, E. Franklin, S.P. Phang, W. Liang, A. Blakers, Excellent ONO passivation on phosphorus and boron diffusion demonstrating a 25% efficient IBC solar cell, Prog. Photovoltaics Res. Appl. 28 (2020) 1034–1044, https://doi.org/10.1002/pip.3310.

[22] J. Melskens, R.J. Theeuwes, L.E. Black, W.J.H. Berghuis, B. Macco, P.C. P. Bronsveld, W.M.M. Kessels, Excellent passivation of n-type silicon surfaces enabled by pulsed-flow plasma-enhanced chemical vapor deposition of phosphorus oxide capped by aluminum oxide, Phys. Status Solidi - Rapid Res. Lett. 15 (2021), 2000399, https://doi.org/10.1002/pssr.202000399.

[23] R.J. Theeuwes, J. Melskens, L.E. Black, W. Beyer, D. Koushik, W.J.H. Berghuis, B. Macco, W.M.M. Kessels, PO_x/Al_2O_3 stacks for c-Si surface passivation: material and interface properties, ACS Appl. Electron. Mater. 3 (2021) 4337–4347, https://doi.org/10.1021/acsaelm.1c00516.

[24] B.W.H. van de Loo, B. Macco, M. Schnabel, M.K. Stodolny, A.A. Mewe, D.L. Young, W. Nemeth, P. Stradins, W.M.M. Kessels, On the hydrogenation of poly-Si passivating contacts by Al_2O_3 and SiN_x thin films, Sol. Energy Mater. Sol. Cells 215 (2020), 110592, https://doi.org/10.1016/j.solmat.2020.110592.

[25] L. Tutsch, F. Feldmann, J. Polzin, C. Luderer, M. Bivour, A. Moldovan, J. Rentsch, M. Hermle, Implementing transparent conducting oxides by DC sputtering on ultrathin SiO_x/poly-Si passivating contacts, Sol. Energy Mater. Sol. Cells 200 (2019), 109960, https://doi.org/10.1016/j.solmat.2019.109960.

[26] B. Macco, D. Deligiannis, S. Smit, R.A.C.M.M. van Swaaij, M. Zeman, W.M. M. Kessels, Influence of transparent conductive oxides on passivation of a-Si:H/c-Si heterojunctions as studied by atomic layer deposited Al-doped ZnO, Semicond. Sci. Technol. 29 (2014), 122001, https://doi.org/10.1088/0268-1242/29/12/122001.

[27] B. Demaurex, S. De Wolf, A. Descoeudres, Z.C. Holman, C. Ballif, Damage at hydrogenated amorphous/crystalline silicon interfaces by indium tin oxide overlayer sputtering, Appl. Phys. Lett. 101 (2012), 171604, https://doi.org/10.1063/1.4764529.

[28] H.B. Profijt, P. Kudlacek, M.C.M. van de Sanden, W.M.M. Kessels, Ion and photon surface interaction during remote plasma ALD of metal oxides, J. Electrochem. Soc. 158 (2011) G88, https://doi.org/10.1149/1.3552663.

[29] Y. Kuang, B. Macco, B. Karasulu, C.K. Ande, P.C.P. Bronsveld, M.A. Verheijen, Y. Wu, W.M.M. Kessels, R.E.I. Schropp, Towards the implementation of atomic layer deposited In_2O_3:H in silicon heterojunction solar cells, Sol. Energy Mater. Sol. Cells 163 (2017), https://doi.org/10.1016/j.solmat.2017.01.011.

[30] A. Cuevas, Y. Wan, D. Yan, C. Samundsett, T. Allen, X. Zhang, J. Cui, J. Bullock, Carrier population control and surface passivation in solar cells, Sol. Energy Mater. Sol. Cells 184 (2018) 38–47, https://doi.org/10.1016/j.solmat.2018.04.026.

[31] T. Longjuan, Z. Yinfang, Y. Jinling, L. Yan, Z. Wei, X. Jing, L. Yunfei, Y. Fuhua, Dependence of wet etch rate on deposition, annealing conditions and etchants for PECVD silicon nitride film, J. Semiconduct. 30 (2009), 096005, https://doi.org/10.1088/1674-4926/30/9/096005.

[32] A. Mameli, B. Karasulu, M.A. Verheijen, B. Barcones, B. Macco, A.J.M. Mackus, W. M.M.E. Kessels, F. Roozeboom, Area-selective atomic layer deposition of ZnO by area activation using electron beam-induced deposition, Chem. Mater. 31 (2019) 1250–1257, https://doi.org/10.1021/acs.chemmater.8b03165.

[33] A.J.M. Mackus, M.J.M. Merkx, W.M.M. Kessels, From the bottom-up: toward area-selective atomic layer deposition with high selectivity, Chem. Mater. 31 (2019) 2–12, https://doi.org/10.1021/acs.chemmater.8b03454.